Applied Nanoscience
https://doi.org/10.1007/s13204-018-0899-1

ORIGINAL ARTICLE

Unsteady squeezing carbon nanotubes based nano-liquid flow with Cattaneo–Christov heat flux and homogeneous–heterogeneous reactions

Dianchen Lu[1] · Zhixiong Li[2,3] · M. Ramzan[1,4,6] · Ahmad Shafee[5] · Jae Dong Chung[6]

Received: 22 August 2018 / Accepted: 16 October 2018

Abstract
The amazing features of carbon nanotubes (CNTs), such as lightweight, high thermal conductivity, good electrical conductivity, mechanical and chemical stability, and physiochemical compatibility, make them highly desirous materials for use in the electrochemical gadgets. Having such magnificent characteristics of carbon nanotubes in mind, our aim in this study is to examine the time-dependent squeezing nanofluid flow of water-based single- and multi-walled carbon nanotubes (SWNTs and MWNTs) in attendance of homogenous–heterogeneous (h–h) reactions between two parallel disks. The present study further comprises the impacts of magnetohydrodynamics (MHD) and Cattaneo–Christov (C–C) heat flux. Numerical solution of ordinary differential equations after engaging apposite transformations is computed. Concentration, temperature, velocity, local Nusselt number, and skin friction coefficient are addressed. Presented analysis reveals that skin friction and Nusselt number show opposite behavior for squeezing parameter Sq for both water-based SWNTs and MWNTs. Furthermore, the velocity field grows for mass transfer parameter. An outstanding consensus is achieved when our presented results are compared with an already studied problem in limiting case. Thus, dependable results are being presented.

Keywords Squeezing flow · Carbon nanotubes · Homogenous–heterogeneous reactions · Cattaneo–Christov heat flux

Introduction

Nanoliquids with exceptional heat transportation characteristics is the most debated subject of today's science owing to their amazing heat transport topographies in comparison to ordinary heat transport fluids (Das et al. 2006; Yu et al. 2007). Nanofluids are characterized as the finest coolant in numerous industries such as optical manufacturing, microelectronics and transportations (Sheikholeslami and Davood Domiri 2015). For heat transport applications, nanofluids possess promising thermophysical features such as thermal conductivity, viscosity, specific heat, and density. The low (density, viscosity) and high (thermal conductivity, specific heat) are the ideal features of efficient coolants as far as heat transport applications are concerned. The available literature pertaining to heat transportation of nano-liquids is primarily based on an improvement in performance of coolants. These coolants can work in different temperature ranges with small viscosity and high thermal conductivity. After the pioneering work of Choi (1995), profuse theoretical and experimental studies (Sheikholeslami and Zeeshan 2017; Sheikholeslami and Houman 2018; Sheikholeslami et al. 2015, 2018a, b; Lu et al. 2018) are presented highlighting various aspects of nano-liquids.

The concept of carbon nanotubes was introduced by Iijima (1991). The CNTs are single or multi-walled, (SWNTs and MWNTs) cylindrical-shaped rolled graphene sheets.

✉ M. Ramzan
mramzan@bahria.edu.pk

1 Department of Mathematics, Faculty of Science, Jiangsu University, Zhenjiang, Jiangsu 212013, China

2 School of Engineering, Ocean University of China, Qingdao 266110, China

3 School of Mechanical, Materials, Mechatronic and Biomedical Engineering, University of Wollongong, Wollongong, NSW 2522, Australia

4 Department of Computer Science, Bahria University, Islamabad Campus, Islamabad 44000, Pakistan

5 Public Authority of Applied Education and Training, College of Technological Studies, Applied Science Department, Shuwaikh, Kuwait

6 Department of Mechanical Engineering, Sejong University, Seoul 143-747, South Korea

Published online: 27 October 2018

Because of their state-of-the-art physicochemical features, and thermal and mechanical characteristics, CNTs are considered as the material of the twenty-first century. Moreover, CNTs are environmentally friendly materials because these are comprised of carbon chains. So, it becomes necessary to examine the features of CNTs on heat transport in fluid flows. Xue (2005) discussed the transport characteristics of CNT-based composites. The heat transfer behavior of nano-liquid flow with CNTs past a horizontal tube is examined by Ding et al. (2006). Lu et al. (2017) described the effects of CNT-based nanofluid with binary chemical reaction, (C–C) heat flux and activation energy. The flow of nano-liquid with CNTs with Marangoni convection and thermal radiation is deliberated by Hayat et al. (2017a). Khan et al. (2017a, b) numerically scrutinized the CNT nano-liquid with slip velocity past two non-parallel walls using the RK–Fehlberg method. Three-dimensional CNT-based nano-liquid flow past a nonlinear stretched surface with (h–h) reaction is discussed by Zakir et al. (2018).

The interesting features of heat transfer in various industrial and engineering applications have expansive demands in fuel cells, transportations, nuclear reactors, drug targeting, cooling towers, microelectronics, etc. In general, thermal conductivity is taken as constant in such procedures. However, logical evidence requires variable features from these properties. A linear change in these properties is observed for fluid metals when the temperature ranges from 0F to 400F (Pal 2013; Vajravelu et al. 2013). The classical Fourier law of heat conduction (20) has been a standard benchmark to measure the heat transfer behavior in numerous practical situations. But owing to parabolic energy equation, the system encountered by an initial disturbance is called paradox in heat conduction. This drawback in the Fourier's model was tackled by Cattaneo (1948) by addition of thermal relaxation time. By doing so, the modified law has produced the hyperbolic energy equation for temperature profile and transportation of heat is allowed to propagate via thermal waves with limited speed. Many practical applications highlighting such heat transportation may be quoted that vary from modeling of skin burn injury to nano-liquid flows [see Tibullo and Zampoli (2011) and Refs. therein]. There are many materials such as sand (21 s), $NaHCO_3$ (29 s) and biological tissues (91–100 s) that possess enough large thermal relaxation time. To maintain the material invariant formulation, Christov (2009) inserted the Oldroyd's upper-convected derivative for time derivative in Maxwell–Cattaneo's model. Now-a-days, this improved model is labelled as C–C heat flux model. Han et al. (2014) instituted the analytical solution of viscoelastic with velocity slip boundary and C–C heat flux. The rotating flow of the upper convected Maxwell fluid with C–C heat flux past a linearly stretched surface is examined numerically and analytically by Mustafa (2015). Khan et al. (2015) deliberated the work of Mustafa for an exponential stretched surface. Hayat et al. (2017b) studied flow of Jeffery fluid past a stretching cylinder with the impacts of stagnation point and C–C heat flux analytically. Lately, Ramzan et al. (2016, 2017) explored 2D Williamson and 3D Maxwell fluid flows with h–h reactions and C–C heat flux models accompanied by convective boundary conditions. Some more recent studies discussing exciting impact of C–C heat flux effect may be seen in Liu et al. (2017), Reddy et al. (2018) and Mustafa et al. (2018).

The presence of h–h reactions in chemical reactions is inevitable. The chemical reaction process in certain cases is relatively slow or even not at all in some cases. To overcome this dilemma in the latter case, the presence of the catalyst is a must. The interaction between these reactions involving reactant species' consumption and the resultant refined product at distinct rates within the liquid and on the surface of the catalyst is very complex. Examples may include combustion, biochemical systems, catalysis, etc. Chaudry and Merkin (1994) deliberated the free convection flow for h–h reactions near the stagnation point. Khan and Pop (2012) also extended the problem of Merkin to the viscoelastic fluid. The case of 2D viscous fluid flow with h–h reactions near a stagnation point past a permeable wall using finite difference method was also considered by Khan and Pop (2010). The problem of nanofluid flow with nanotubes considering the effects of Newtonian heating with h–h reactions is studied by Hayat et al. (2015). Hayat et al. (2016a, 2016b, 2016c, 2016d) also deliberated the combination of h–h reactions with C–C heat flux with different fluid combinations. Khan et al. (2017) investigated the 3D Sisko fluid flow with effects of h–h reactions with C–C heat flux.

A literature survey indicates that abundant research articles are available pertaining to nanofluid flows with combined impacts of the h–h reactions and C–C heat flux past linear/nonlinear/curved stretching surfaces. Comparatively, less research work is done with nanotubes and as far as our knowledge is concerned no study so far is conducted for the nano-liquid squeezing flow with CNTs between two disks with impacts of both h–h reactions with C–C heat flux. Thus, our prime objective is to examine the water (base) nano-liquid flow with SWNTs and MWNTs past two disks with impacts of C–C heat flux and h–h reaction. Numerical solution of the subject model is acquired utilizing bvp4c function of the MAPLE software. Influence of arising parameters on Nusselt number and skin friction are depicted through graphical illustrations with the requisite discussion.

Mathematical modeling

Consider an unsteady, incompressible two-dimensional MHD water-based nanoparticle flow amid two infinitely parallel disks having a distance $z = h(t) = H(1 - \alpha t)^{0.5}$. We have considered nanoparticles of two kinds, SWCNTs and

MWCNTs, with the base fluid, i.e., water. Moreover, the magnetic field $B_0(1-\alpha t)^{-0.5}$ is directed in the normal direction to the disks. The induced magnetic field is not considered because we have taken small Reynolds number. Here, the temperature T_h refers to the upper disk $z = h(t)$ and T_w for the lower disk $z = 0$. Furthermore, the upper disk $z = h(t)$ is moving to and fro from the immobile and permeable lower disk $z = 0$ with the velocity $\frac{dh}{dt}$. The physical sketch of the presented model is plotted in Fig. 1.

The model for homogeneous (isothermal cubic autocatalytic) and heterogeneous reactions with two chemical species A^* and B^* proposed by Merkin and Chudhary (1994) is given by

$$A^* + 2B^* \rightarrow 3B^*, \quad \text{rate} = k_c a b^2, \tag{1}$$

$$A^* \rightarrow B^*, \quad \text{rate} = k_s a, \tag{2}$$

where concentrations for the chemical species B^* and A^* are symbolized by b and a and k_j, $(j = c, s)$ are the rate quantities. Both reaction forms are supposed to be isothermal. Applying the boundary layer estimation, the governing equations of the problem can be stated as

$$\frac{\partial u}{\partial r} + \frac{u}{r} + \frac{\partial w}{\partial z} = 0, \tag{3}$$

$$\frac{\partial u}{\partial t} + u\frac{\partial u}{\partial r} + w\frac{\partial u}{\partial z} = -\frac{1}{\rho_{\text{nf}}}\frac{\partial p}{\partial r} + \frac{\mu_{\text{nf}}}{\rho_{\text{nf}}}\left(\frac{\partial^2 u}{\partial r^2} + \frac{1}{r}\frac{\partial u}{\partial r} - \frac{u}{r^2} + \frac{\partial^2 u}{\partial z^2}\right) - \frac{\sigma}{\rho_{\text{nf}}}B^2(t)u, \tag{4}$$

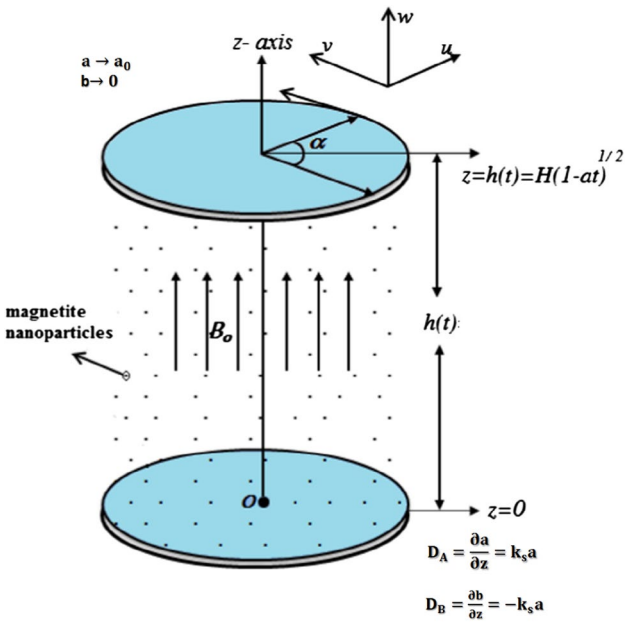

Fig. 1 Physical diagram of the problem

$$\frac{\partial w}{\partial t} + u\frac{\partial w}{\partial r} + w\frac{\partial w}{\partial z} = -\frac{1}{\rho_{\text{nf}}}\frac{\partial p}{\partial z} + \frac{\mu_{\text{nf}}}{\rho_{\text{nf}}}\left(\frac{\partial^2 w}{\partial r^2} + \frac{1}{r}\frac{\partial w}{\partial r} + \frac{\partial^2 w}{\partial z^2}\right), \tag{5}$$

$$\frac{\partial T}{\partial t} + u\frac{\partial T}{\partial r} + w\frac{\partial T}{\partial z} + \varepsilon\left(\frac{\partial^2 T}{\partial t^2} + \frac{\partial u}{\partial t}\frac{\partial T}{\partial r} + 2u\frac{\partial^2 T}{\partial t \partial r} + 2w\frac{\partial^2 T}{\partial t \partial z} + \frac{\partial w}{\partial t}\frac{\partial T}{\partial z} + u\frac{\partial u}{\partial r}\frac{\partial T}{\partial r} + w\frac{\partial w}{\partial z}\frac{\partial T}{\partial z} + u\frac{\partial w}{\partial r}\frac{\partial T}{\partial z} + w\frac{\partial u}{\partial z}\frac{\partial T}{\partial r} + 2uw\frac{\partial^2 T}{\partial r \partial z} + u^2\frac{\partial^2 T}{\partial r^2} + w^2\frac{\partial^2 T}{\partial z^2}\right) = \frac{k_{nf}}{(\rho C_p)_{nf}}\left(\frac{\partial^2 T}{\partial r^2} + \frac{1}{r}\frac{\partial T}{\partial r} + \frac{\partial^2 T}{\partial z^2}\right), \tag{6}$$

$$\frac{\partial a}{\partial t} + u\frac{\partial a}{\partial r} + w\frac{\partial a}{\partial z} = D_A\left(\frac{\partial^2 a}{\partial r^2} + \frac{1}{r}\frac{\partial a}{\partial r} + \frac{\partial^2 a}{\partial z^2}\right) - k_c a b^2, \tag{7}$$

$$\frac{\partial b}{\partial t} + u\frac{\partial b}{\partial r} + w\frac{\partial b}{\partial z} = D_B\left(\frac{\partial^2 b}{\partial r^2} + \frac{1}{r}\frac{\partial b}{\partial r} + \frac{\partial^2 b}{\partial z^2}\right) + k_c a b^2, \tag{8}$$

where D_A and D_B are the diffusion coefficients corresponding to the chemical species A^* and B^*. The appropriate boundary conditions are specified by

$$\begin{aligned} &u = 0, \quad w = \frac{dh}{dt}, \quad T = T_h, \quad a \rightarrow a_0, \quad b \rightarrow 0, \quad \text{at } z = h(t), \\ &u = 0, \quad w = -\frac{w_0}{\sqrt{1-\alpha t}}, \quad T = T_w, \quad D_A\frac{\partial a}{\partial z} = k_s a, \\ &D_B\frac{\partial b}{\partial z} = -k_s a \quad \text{at } z = 0. \end{aligned} \tag{9}$$

The thermophysical traits (specific heat, density and thermal conductivity) of the base fluid (water) and carbon nanotubes (SWCNTs and MWCNTs) are given in Table 1.

The mathematical form for the thermophysical properties are

$$\mu_{\text{nf}} = \frac{\mu_f}{(1-\phi)^{2.5}}, \quad \nu_{\text{nf}} = \frac{\mu_{\text{nf}}}{\rho_{\text{nf}}},$$

$$\rho_{\text{nf}} = (1-\phi)\rho_f + \phi\rho_{CNT}, \quad \frac{k_{\text{nf}}}{k_{\text{f}}} = \frac{(1-\phi) + 2\phi\frac{k_{\text{CNT}}}{k_{\text{CNT}}-k_{\text{f}}}\ln\frac{k_{\text{CNT}}+k_{\text{f}}}{2k_f}}{(1-\phi) + 2\phi\frac{k_{\text{f}}}{k_{\text{CNT}}-k_{\text{f}}}\ln\frac{k_{\text{CNT}}+k_{\text{f}}}{2k_{\text{f}}}}, \tag{10}$$

Table 1 Thermophysical characteristics of the base fluids and CNTs

Physical properties	Base fluid (water)	Nanoparticle (MWCNTs)	Nanoparticle (SWCNTs)
C_p (J/kg k)	4179.00	796	425
ρ (kg/m^3)	997.100	1600	2600
k (W/mk)	0.61300	3000	6600

where μ_f, μ_{nf}, ϕ, $\phi\rho_{CNT}$, ρ_f, ρ_{nf}, k_{CNT}, k_{nf}, and k_f denote dynamic viscosity of the fluid, dynamic viscosity of the nanofluid, volume fraction of the nanoparticle, volume fraction of the carbon nanotubes, density of the fluid, nanofluid's density, nanotubes thermal conductivity, thermal conductivity of the nanofluid and the base fluid's thermal conductivity, respectively.

Similarity transformation

The following non-dimensional transformation was used to change the above nonlinear partial differential equations to dimensionless ordinary differential form, i.e.,

$$u = \frac{\alpha r}{2(1-\alpha t)} f'(\eta), \quad w = -\frac{\alpha H}{(1-\alpha t)^{\frac{1}{2}}} f(\eta),$$
$$B(t) = \frac{B_0}{(1-\alpha t)^{\frac{1}{2}}}, \quad \eta = \frac{z}{H(1-\alpha t)^{\frac{1}{2}}}, \quad \theta = \frac{T-T_h}{T_w - T_h}. \tag{11}$$

Continuity equation is automatically satisfied, and Eqs. (4)–(9) become

$$\frac{1}{(1-\phi)^{2.5}} f'''' - S_q\left((1-\phi) + \phi\frac{\rho_s}{\rho_f}\right)\left(\eta f''' + 3f'' - 2ff''\right) - Mf'' = 0, \tag{12}$$

$$\frac{k_{nf}}{k_f}\theta'' + S_q \Pr\left((1-\phi) + \phi\frac{(\rho C_p)_s}{(\rho C_p)_f}\right)\left[2f\theta' - \eta\theta' - \gamma\left(\eta^2\theta'' - 2\eta f\theta'' - \eta f'\theta' + ff'\theta' + f^2\theta''\right)\right] = 0, \tag{13}$$

$$\frac{1}{S_c}h'' - \frac{\eta}{2}h' + fh' - k1hg^2 = 0, \tag{14}$$

$$\frac{\delta}{S_c}g'' - \frac{\eta}{2}g' + fg' + k1hg^2 = 0, \tag{15}$$

with

$$f(0) = s, \quad f'(0) = 0, \quad \theta(0) = 1, h'(0) = k2\, h(0),$$
$$\delta g'(0) = -ks = h(0),$$
$$f(1) = 1/2, \quad f'(1) = 0, \quad \theta(1) = 0, \quad h(1) \to 1, \quad g(1) \to 0, \tag{16}$$

where prime designates the derivative w.r.t η. $S_q = \frac{\alpha H^2}{2\nu_f}$ signifies the squeeze number, $M = \sqrt{\frac{\sigma {B_0}^2 H^2}{\alpha\rho_f}}$ the Hartmann number, $Pr = \frac{\mu_f(\rho C_p)_f}{\rho_{fk_f}}$ the Prandtl number, $s = \frac{w_0}{\alpha H}$ the suction parameter, $\gamma = \frac{\varepsilon\alpha}{2(1-at)}$ is the thermal relaxation parameter, $S_c = \frac{\alpha H^2}{D_A}$ the Schmidt number, $k1 = \frac{k_c {a_0}^2(1-\alpha t)}{\alpha}$ the measure of strength of homogeneous reaction, $\delta = \frac{D_B}{D_A}$ the quotient of diffusion coefficient and $k2 = \frac{k_s}{D_A}H(1-\alpha t)$ is the measure of strength of heterogeneous reaction.

In general, the chemical species B^* and A^* will not be identical, but we can anticipate that these will be analogous in size. In such a case, we suppose that the diffusion species coefficients D_B and D_A are alike, i.e., $\delta = 1$, thus we have

$$h(\eta) + g(\eta) = 1. \tag{17}$$

Now applying the above property, Eqs. (14) and (15) and their corresponding boundary conditions take the form

$$\frac{1}{S_c}h'' - \frac{\eta}{2}h' + fh' - k1h(1-h)^2 = 0, \tag{18}$$

$$h'(0) = k2\, h(0), \qquad h(1) \to 1. \tag{19}$$

Friction factor and local Nusselt number

The dimensional form of the C_{fr} (skin friction coefficient) and Nu (the local Nusselt number) is categorized as

$$C_f = \frac{\mu_{nf}\left(\frac{\partial u}{\partial z} + \frac{\partial w}{\partial r}\right)_{z=h(t)}}{\rho_f\left(-\alpha H/2\sqrt{1-\alpha t}\right)^2}, \quad Nu = \frac{k_{nf}(\rho C_p)_f}{\rho_f k_f}. \tag{20}$$

Using Eq. (11) in Eq. (20), we acquire

$$\frac{H^2}{r^2}Re_r C_{fr} = \frac{1}{\frac{1}{(1-\phi)^{2.5}}\left((1-\phi) + \phi\frac{\rho_s}{\rho_f}\right)} f''(1),$$
$$(1-\alpha t)^{1/2} Nu = -\frac{k_{nf}}{k_f}\theta'(1), \tag{21}$$

where $Re_r = \frac{\rho_f r\alpha H(1-\alpha t)^{1/2}}{2\mu_f}$ is the local squeezed Reynolds number.

Results and discussion

To discuss the fluid flow behavior and heat transfer, results are sketched for axial velocity $f(\eta)$, radial velocity $f'(\eta)$, and temperature profile $\theta(\eta)$ and for concentration field $h(\eta)$ for distinct values of flow parameters say squeezing parameter S_q, Hartmann number M, the suction parameter s, the homogeneous reaction parameter $k1$, the thermal relaxation parameter γ, the Schmidt number S_c and the heterogeneous reaction parameter $k2$. For this, we fixed different flow parameters' values as $s = 0.4$, $M = 0.5$, $Sq = 1.0$, $Pr = 6.2$, $\gamma = 0.5$, $\phi = 0.1$, $k1 = 0.7 = k2$, $Sc = 1.0$. The outcomes are acquired for both single-walled carbon nanotubes (SWCNTs) and multi-walled carbon nanotubes (MWCNTs). Figure 2 shows the effect of suction parameter s on axial

velocity $f(\eta)$. It can be seen that the axial velocity increases for higher rate of mass transfer parameter s. It is a known fact that for high suction, velocity profile escalates, which results in reverse flow. The effect of reverse flow is more dominating near the upper plate in comparison to the lower one. The pressure gradient is the root cause to create the reverse flow near the lower plate and because of this fact big number of fluid particles move away from the lower plate. Figure 3 is sketched for the velocity profile $f'(\eta)$ versus squeezing parameter S_q. This figure shows that for contraction of disks, i.e., $S_q = -1, \ -2, \ -3$, the velocity profile increases for both single-walled carbon nanotubes (SWCNTs) and multi-walled carbon nanotubes (MWCNTs), while an opposite behavior can be observed for $S_q = 1, \ 2, \ 3$ when disks are moving far from each other. The impact of suction parameter s for both SWCNTs and MWCNTs are portrayed in Figs. 4 and 5. Figure 4 emphasizes that for higher value of mass transfer parameter, the velocity profile $f'(\eta)$ declines for MWCNTs. It is observed that whenever suction effect is overwhelming, velocity profile decreases. The same behavior can be seen for SWCNTs in Fig. 5. To see the impact of nanoparticle volume friction, results are sketched in Fig. 6. In the presence of MWCNTs and SWCNTs, it is remarked that the velocity reduces in some areas close to the disk for growing values of nanoparticle volume friction ϕ but after a certain distance from the disk, this profile starts developing until the far-field boundary condition is asymptotically satisfied. This impact can be visualized in Fig. 6. However, for incremental values of nanoparticle volume friction ϕ in case of squeezing flow, the temperature declines in Fig. 7 for both cases. The behavior of dimensionless temperature profile for sundry values of squeezing parameter S_q and thermal

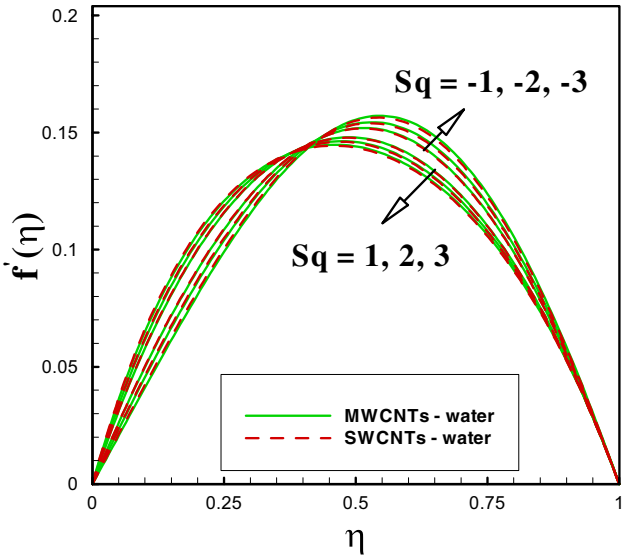

Fig. 3 Velocity profile for Sq

relaxation parameter γ, respectively, for both SWCNTs and MWCNTs, is represented in Figs. 8 and 9. In Fig. 8, it is examined that the temperature demonstrates reducing behavior within the domain $0 < \eta < 0.3$ when $S_q = -1, -2, -3$, i.e., when the disks are contracting. However, it depicts an increasing tendency in the region $0.3 < \eta \leq 1$, for higher values of squeezing parameter $S_q = 1, \ 2, \ 3$ that is when the disks are moving far from each other. To see the effect of thermal relaxation parameter γ on temperature profile $\theta(\eta)$, results are sketched in Fig. 9. It is observed that the higher rate of γ causes augmentation in the temperature profile $\theta(\eta)$

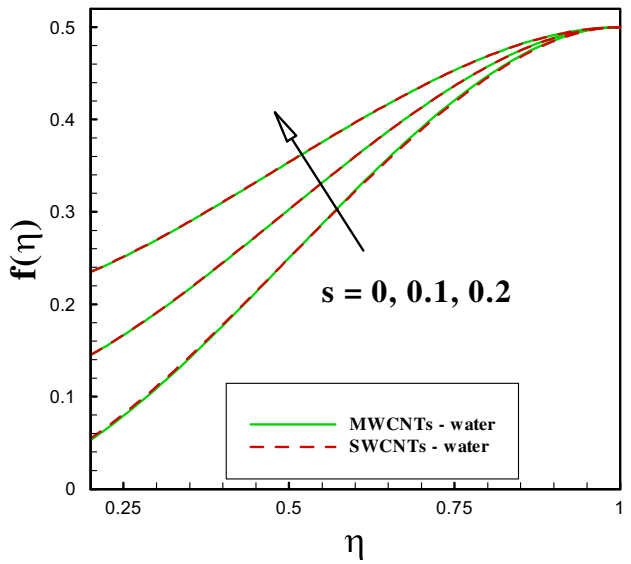

Fig. 2 Axial velocity for s

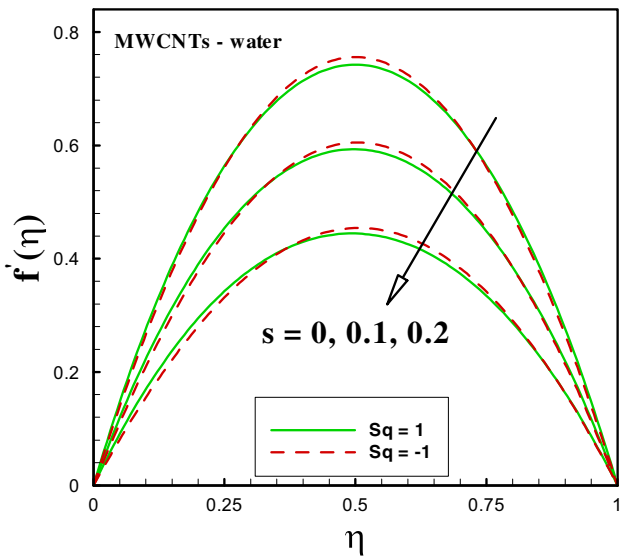

Fig. 4 Velocity profile for s in case of MWCNTs

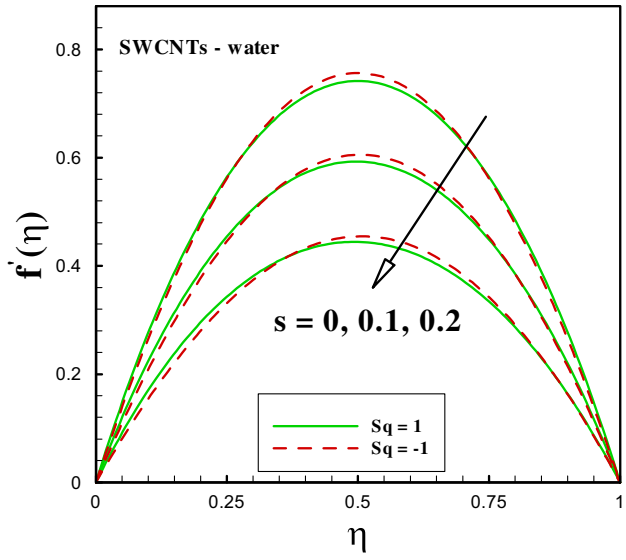

Fig. 5 Velocity profile for s in case of SWCNTs

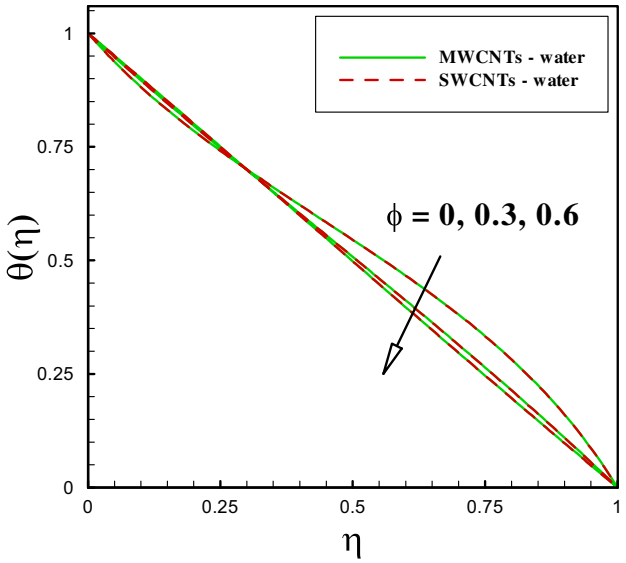

Fig. 7 Temperature profile for ϕ

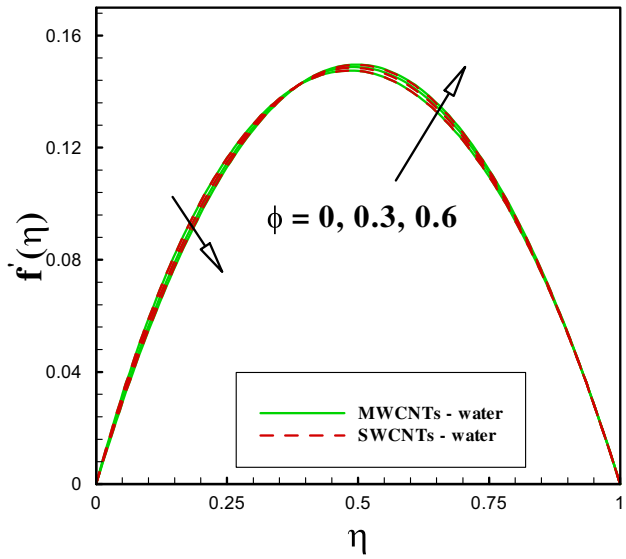

Fig. 6 Velocity profile for ϕ

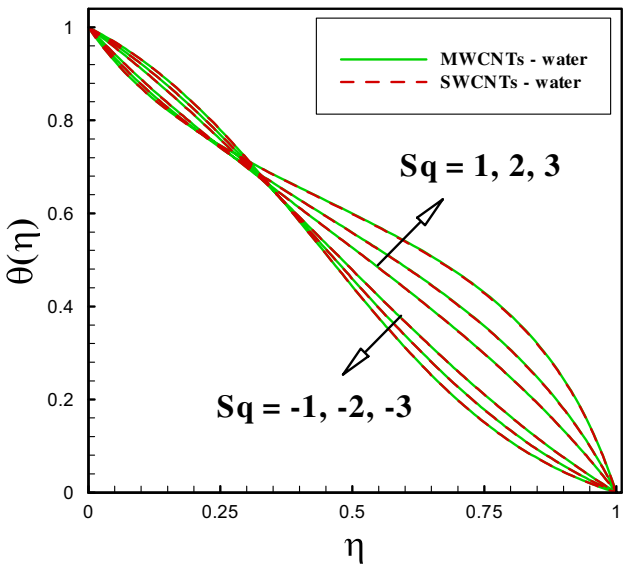

Fig. 8 Temperature profile for Sq

for both SWNTs and MWNTs. To discuss concentration field $h(\eta)$ with respect to homogeneous reaction parameter $k1$, heterogeneous reaction parameter $k2$ and the Schmidt number S_c, respectively, results are plotted in Figs. 10, 11, and 12 for both SWCNTs and MWCNTs. Figure 10 indicates that for growing values of homogeneous reaction parameter, concentration profile $h(\eta)$ reduces as the reactants are consumed during the homogeneous reaction which ultimately declines the concentration. The similar result is seen in Fig. 11 for heterogeneous reaction parameter. Figure 12 portrays the influence of Schmidt number S_c on concentration field $h(\eta)$. It is witnessed that for higher values of Schmidt number, reduction in $h(\eta)$ is monitored. As Schmidt number is the quotient of momentum to mass diffusivity, smaller mass diffusivity relates to stronger Schmidt number which ultimately decreases the concentration of the fluid.

To illustrate the skin friction $\frac{H^2}{r^2}Re_rC_{fr}$, rate of heat transfer $(1-\alpha t)^{1/2}Nu$ and surface concentration $h(0)$, we plotted for both water-based SWCNTs and MWCNTs in Figs. 13, 14, 15, and 16. The variation of squeezing parameter S_q for the skin friction and the Nusselt number against mass transfer parameter s are discussed in Figs. 13 and 14. It

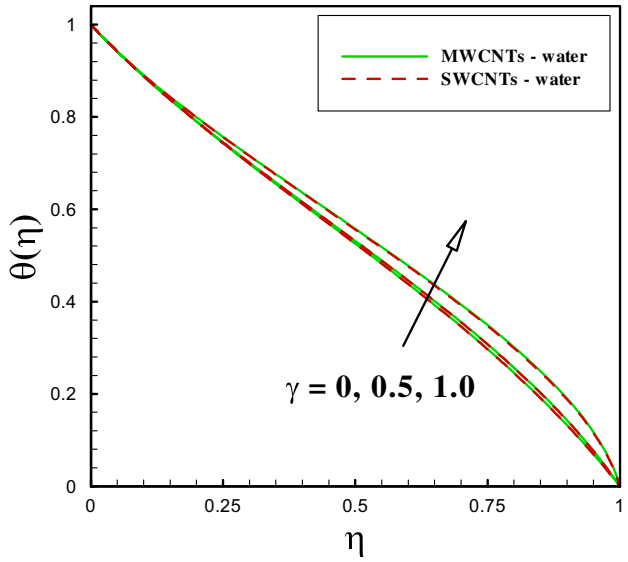

Fig. 9 Temperature profile for γ

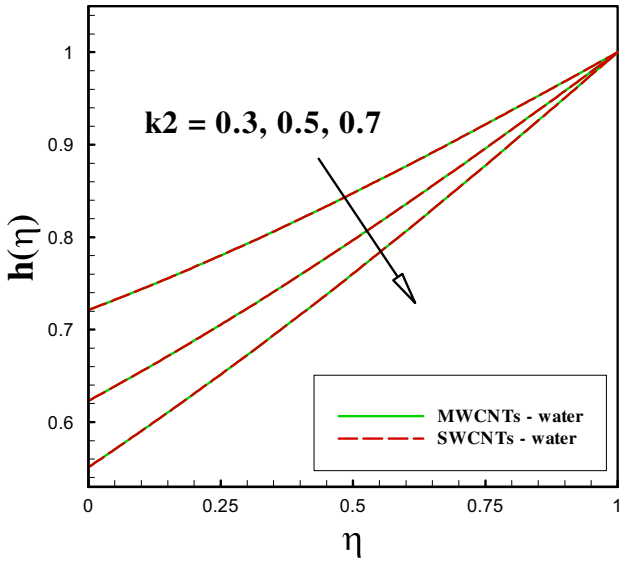

Fig. 11 Concentration profile for $k2$

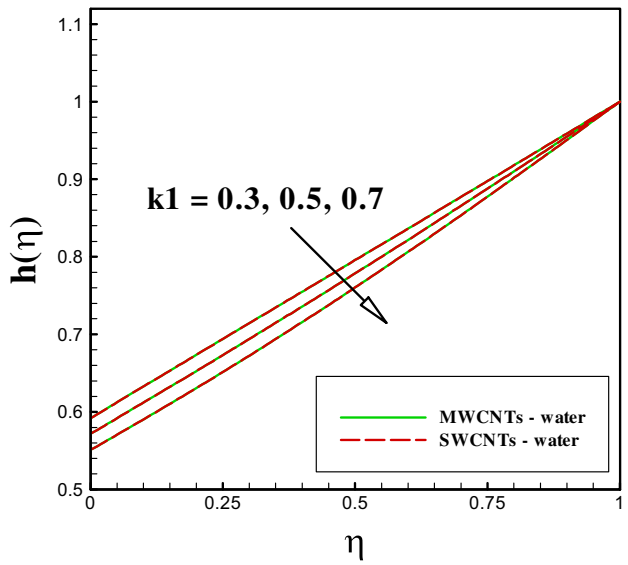

Fig. 10 Concentration profile for $k1$

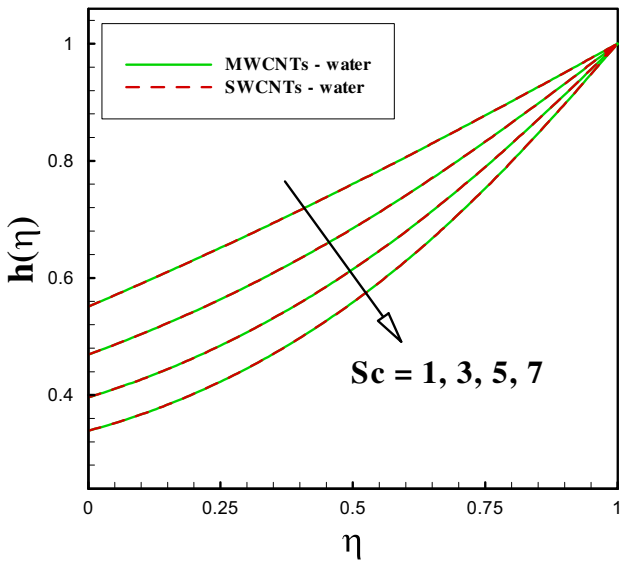

Fig. 12 Concentration profile for S_c

can be perceived that for the increasing value of squeezing parameter $S_q = -1,\ 0,\ 1$, the skin friction coefficient reduces. While for the rate of heat transfer, an opposite trend is observed. From Figs. 15 and 16, the variation of thermal relaxation parameter γ against squeezing parameter S_q is sketched in the presence and absence of nanoparticle concentration ϕ. It is observed that for increasing value of γ, the rate of heat transfer for MWCNTs also improves as depicted in Fig. 15. For SWCNTs, similar results can be seen for the rate of heat transfer (see Fig. 16). For the surface concentration $h(0)$, the effects of homogeneous reaction parameter $k1$ and heterogeneous reaction parameter $k2$ are shown in Figs. 17 and 18. It is perceived that with the increment of $k1 = 0.3,\ 0.5,\ 0.7$ with respect to $k2$, $h(0)$ reduces in Fig. 17 for both cases. Moreover, for the heterogeneous reaction parameter $k2$, the surface concentration decreases against $k1$ (Fig. 18).

Table 2 characterizes the comparison of skin friction coefficient with Haq et al. (2016) for the varied values of S_q and M in the absence of suction and solid volume fraction of nanoparticles. An excellent concurrence is achieved in this regard. Hence, trustworthy results are being presented.

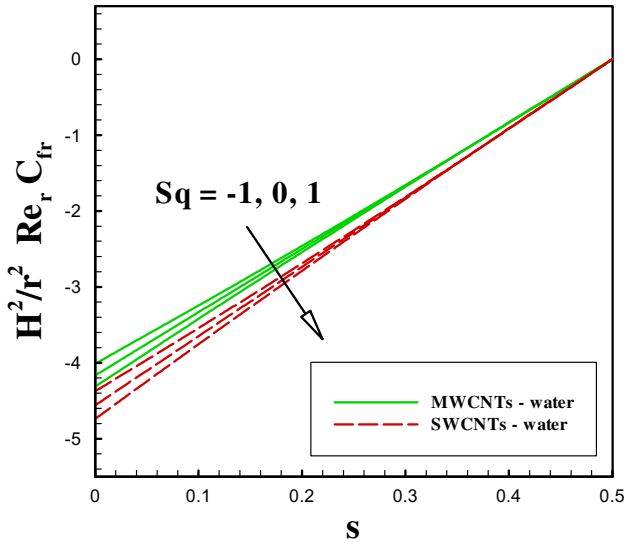

Fig. 13 Fig. 13 Skin friction for S_q

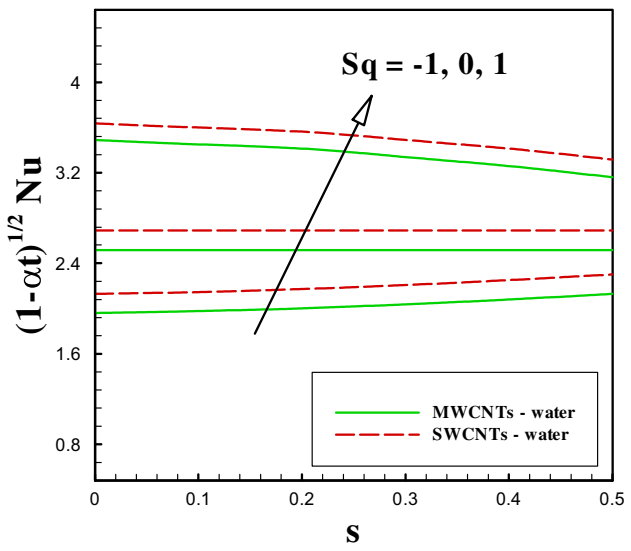

Fig. 14 Nusselt number for S_q

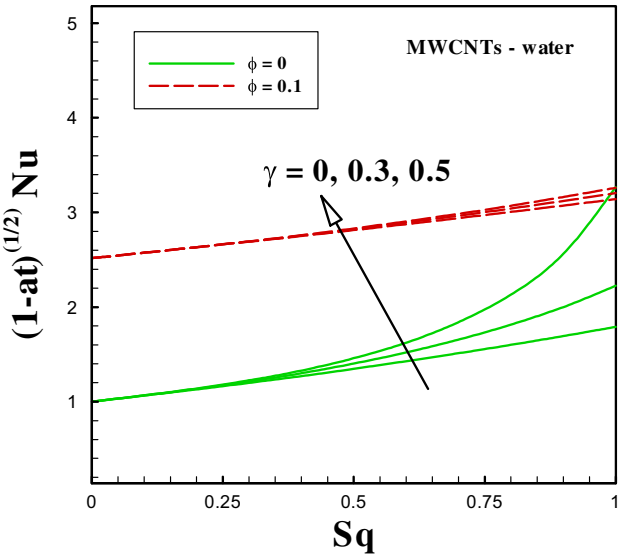

Fig. 15 Nusselt number for γ in case of MWCNTs

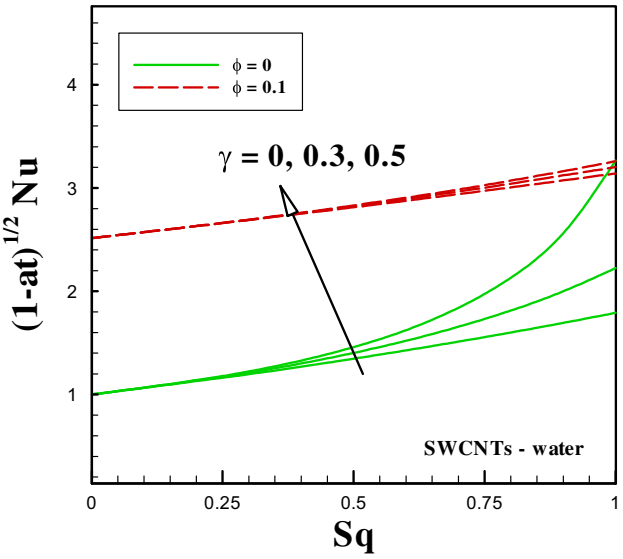

Fig. 16 Nusselt number for γ in case of SWCNTs

Final remarks

Throughout this study, squeezing nano-liquid flow comprising CNTs (SWNTs and MWNTs) with Cattaneo–Christov heat flux is examined numerically. Additional impacts of MHD and homogenous–heterogeneous reactions are also taken into account. Results for both SWNTs and MWNTs are constructed. Prominent impacts of arising parameters for both SWNTs and MWNTs versus involved distributions are illustrated graphically and debated accordingly. Concluding remarks for the whole analysis are presented as under:

- Skin friction and Nusselt number exhibit opposite trend for squeezing parameter *Sq* for both

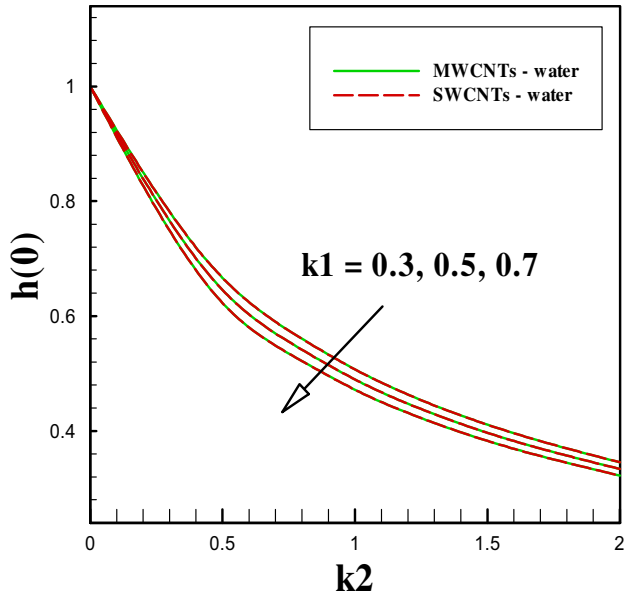

Fig. 17 Surface concentration for $k1$ and $k2$

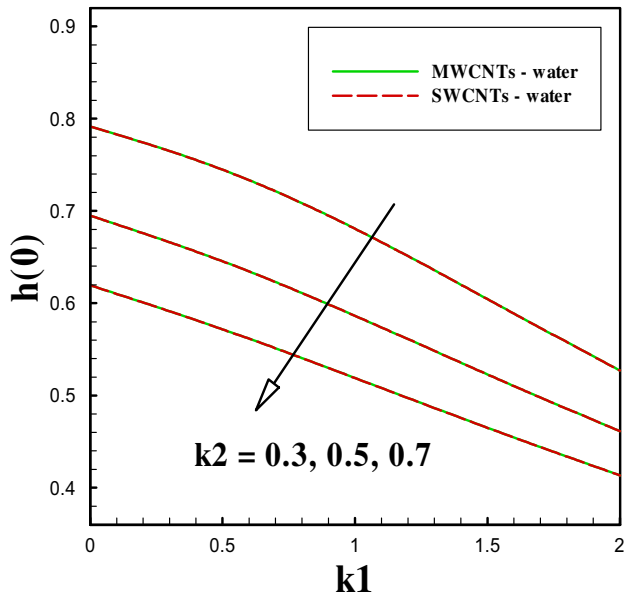

Fig. 18 Surface concentration for $k2$ and $k1$

water-based SWNTs, and MWNTs.

- For both SWNTs and MWNTs, velocity distribution increases versus mass transfer parameter s.
- The concentration profile declines for both homogenous–heterogeneous reactions in case of SWNTs and MWNTs.
- The temperature profile shows opposite behavior for nanoparticle volume friction ϕ and thermal relaxation parameter γ.

Table 2 Numerically calculated values of skin friction for varied values of S_q and M when compared with Haq et al. (2016)

S_q	M	$\frac{1}{(1-\phi)^{2.5}\left(1-\phi+\phi\frac{\rho_s}{\rho_f}\right)}f''(1)$	Haq et. al (2016)
0.5	0.0	−3.1461941	−3.14619
	1.0	−3.1940816	−3.19408
	2.0	−3.2413602	−3.24136
−1.0	1.0	−2.7596174	−2.75962
0.0		−3.0496468	−3.04965
1.0		−3.3381297	−3.33813

Compliance with ethical standards

Conflict of interest Authors have no conflict of interest regarding this publication.

References

Cattaneo C (1948) Sulla conduzione del calore. Atti Sem Mat Fis Univ Modena 3:83–101

Chaudhary MA, Merkin JH (1994) Free-convection stagnation-point boundary layers driven by catalytic surface reactions: I the steady states. J Eng Math 28(2):145–171

Choi SUS, Estman JA (1995) Enhancing thermal conductivity of fluids with nanoparticles. ASME Publ Fed 231:99–106

Christov CI (2009) On frame indifferent formulation of the Maxwell–Cattaneo model of finite-speed heat conduction. Mech Res Commun 36(4):481–486

Das SK, SUS Choi, Patel HE (2006) Heat transfer in nanofluids—a review. Heat Transf Eng 27(10):3–19

Ding Y, Alias H, Wen D, Richard A, Williams (2006) Heat transfer of aqueous suspensions of carbon nanotubes (CNT nanofluids). Int J Heat Mass Transf 49(1–2):240–250

Fourier J (1822) Theorie analytique de la chaleur, par M. Fourier. Chez Firmin Didot, père et fils

Gnaneswara RM, Sudha Rani MVVNL, Ganesh Kumar K, Prasannakumara BC (2018) Cattaneo–Christov heat flux and non-uniform heat-source/sink impacts on radiative Oldroyd-B two-phase flow across a cone/wedge. J Braz Soc Mech Sci Eng 40(2):95

Han S, Zheng L, Li C, Zhang X (2014) Coupled flow and heat transfer in viscoelastic fluid with Cattaneo–Christov heat flux model. Appl Math Lett 38:87–93

Haq R, Ul NFM, Noor, Khan ZH (2016) Numerical simulation of water based magnetite nanoparticles between two parallel disks. Adv Powder Technol 27(4):1568–1575

Hayat T, Farooq M, Alsaedi A (2015) Homogeneous-heterogeneous reactions in the stagnation point flow of carbon nanotubes with Newtonian heating. AIP Adv 5(2):027130

Hayat T, Qayyum S, Imtiaz M, Alsaedi A (2016a) Impact of Cattaneo–Christov heat flux in Jeffrey fluid flow with homogeneous-heterogeneous reactions. PloS one 11(2):e0148662

Hayat T, Ijaz Khan M, Farooq M, Alsaedi A, Waqas M, Yasmeen T (2016b) Impact of Cattaneo–Christov heat flux model in flow of variable thermal conductivity fluid over a variable thicked surface. Int J Heat Mass Transf 99:702–710

Hayat T, Imtiaz M, Alsaedi A, Almezal S (2016c) On Cattaneo–Christov heat flux in MHD flow of Oldroyd-B fluid with homogeneous–heterogeneous reactions. J Magn Magn Mater 401:296–303

Hayat T, Ijaz Khan M, Farooq M, Yasmeen T, Alsaedi A (2016d) Stagnation point flow with Cattaneo–Christov heat flux and homogeneous-heterogeneous reactions. J Mol Liq 220:49–55

Hayat T, Ijaz Khan M, Farooq M, Alsaedi A, Yasmeen T (2017a) Impact of Marangoni convection in the flow of carbon–water nanofluid with thermal radiation. Int J Heat Mass Transf 106:810–815

Hayat T, Khan MI, Farooq M, Alsaedi A, Khan MI (2017b) Thermally stratified stretching flow with Cattaneo–Christov heat flux. Int J Heat Mass Transf 106:289–294

Hussain ZT, Hayat A, Alsaedi, Ahmad B (2018) Three-dimensional convective flow of CNTs nanofluids with heat generation/absorption effect: a numerical study. Comput Methods Appl Mech Eng 329:40–54

Iijima S (1991) Helical microtubules of graphitic carbon. Nature 354(6348):56

Khan WA, Pop I (2010) Flow near the two-dimensional stagnation-point on an infinite permeable wall with a homogeneous–heterogeneous reaction. Commun Nonlinear Sci Numer Simul 15(11):3435–3443

Khan WA, Pop IM (2012) Effects of homogeneous–heterogeneous reactions on the viscoelastic fluid toward a stretching sheet. J Heat Transf 134(6):064506

Khan J, Ahmad M, Mustafa T, Hayat, Alsaedi A (2015) Numerical study of Cattaneo–Christov heat flux model for viscoelastic flow due to an exponentially stretching surface. PLOS One 10(9):e0137363

Khan U, Ahmed N, Mohyud-Din ST (2017a) Heat transfer effects on carbon nanotubes suspended nanofluid flow in a channel with non-parallel walls under the effect of velocity slip boundary condition: a numerical study. Neural Comput Appl 28(1):37–46

Khan M, Ahmad L, Khan WA, Alshomrani AS, Alzahrani AK, Alghamdi MS (2017b) A 3D Sisko fluid flow with Cattaneo–Christov heat flux model and heterogeneous-homogeneous reactions: a numerical study. J Mol Liq 238:19–26

Liu L, Zheng L, Liu F, Zhang X (2017) Heat conduction with fractional cattaneo–christov upper-convective derivative flux model. Int J Therm Sci 112:421–426

Lu DM, Ramzan S, Ahmad JD, Chung, Farooq U (2017) Upshot of binary chemical reaction and activation energy on carbon nanotubes with Cattaneo–Christov heat flux and buoyancy effects. Phys Fluids 29(12):123103

Lu D, Ramzan M, Ahmad S, Chung JD, Farooq U (2018) A numerical treatment of MHD radiative flow of Micropolar nanofluid with homogeneous-heterogeneous reactions past a nonlinear stretched surface. Sci Rep 8(1):12431

Mustafa M (2015) Cattaneo–Christov heat flux model for rotating flow and heat transfer of upper-convected Maxwell fluid. AIP Adv 5(4):047109

Mustafa M, Hayat T, Alsaedi A (2018) Heat transfer in Oldroyd-B fluid flow due to an exponentially stretching wall utilizing Cattaneo–Christov heat flux model. J Braz Soc Mech Sci Eng 40(4):191

Pal D, Chatterjee S (2013) Soret and Dufour effects on MHD convective heat and mass transfer of a power-law fluid over an inclined plate with variable thermal conductivity in a porous medium. Appl Math Comput 219(14):7556–7574

Ramzan M, Bilal M, Jae Dong C (2016) Effects of MHD homogeneous-heterogeneous reactions on third grade fluid flow with Cattaneo–Christov heat flux. J Mol Liq 223:1284–1290

Ramzan M, Bilal M, Chung JD (2017) Influence of homogeneous-heterogeneous reactions on MHD 3D Maxwell fluid flow with Cattaneo–Christov heat flux and convective boundary condition. J Mol Liq 230:415–422

Sheikholeslami M, Davood Domiri G (2015) Nanofluid flow and heat transfer between parallel plates considering Brownian motion using DTM. Comput Methods Appl Mech Eng 283:651–663

Sheikholeslami M, Houman B (2018) Rokni. "Numerical simulation for impact of Coulomb force on nanofluid heat transfer in a porous enclosure in presence of thermal radiation. Int J Heat Mass Transf 118:823–831

Sheikholeslami M, Zeeshan A (2017) Analysis of flow and heat transfer in water based nanofluid due to magnetic field in a porous enclosure with constant heat flux using CVFEM. Comput Methods Appl Mech Eng 320:68–81

Sheikholeslami M, Hatami M, Domairry G (2015) Numerical simulation of two phase unsteady nanofluid flow and heat transfer between parallel plates in presence of time dependent magnetic field. J Taiwan Inst Chem Eng 46:43–50

Sheikholeslami M, Shehzad SA, Li Z, Shafee A (2018a) Numerical modeling for alumina nanofluid magnetohydrodynamic convective heat transfer in a permeable medium using Darcy law. Int J Heat Mass Transf 127:614–622

Sheikholeslami M, Shafee A, Ramzan M, Li Z (2018b) Investigation of Lorentz forces and radiation impacts on nanofluid treatment in a porous semi annulus via Darcy law. J Mol Liq 272:8–14

Tibullo V, Zampoli V (2011) A uniqueness result for the Cattaneo–Christov heat conduction model applied to incompressible fluids. Mech Res Commun 38(1):77–79

Vajravelu K, Prasad KV, Chiu-On N (2013) Unsteady convective boundary layer flow of a viscous fluid at a vertical surface with variable fluid properties. Nonlinear Anal Real World Appl 14(1):455–464

Xue QZ (2005) Model for thermal conductivity of carbon nanotube-based composites. Physica B 368(1–4):302–307

Yu W, France DM, Stephen US, Choi, Routbort JL (2007) Review and assessment of nanofluid technology for transportation and other applications. No. ANL/ESD/07–9. Argonne National Lab.(ANL), Argonne, IL (United States),